6
Artigos em Congressos

F. C. Fávero, S. M. M. Quintero, C. Martelli, A. B. Braga and I. C. S. Carvalho, "Thermal response evaluation of a special fiber sensor"XXXII Encontro Nacional da Matéria Condensada, Águas de Lindóia, Brasil, 2009

F. C. Fávero, S. M. M. Quintero, Vinícius V. Silva, C. Martelli, A. M. B. Braga, I.C. S. Carvalho and R. W. A. Llerena; "Photonic crystal fiber pressure sensor."Optical Fiber Sensor 20, Edinburgh, UK, 2009

G. A. Cardenas-Sevilla, F. C. Favero, V. Finazzi, J. Villatoro, V. Pruneri; "Functional photonic crystal fiber devices based on modes overlapping", Optoel 2011, Santander, Spain.

G. A. Cárdenas-Sevilla, F. C. Favero, V. Finazzi, J. Villatoro, V. Pruneri; "High-visibility photonic crystal fiber interferometer for ultrasensitive refractometric sensing", ICO-22, Puebla, Mexico, 2011.

F. C. Favero, Isabel C. S. Carvalho, Arthur M. B. Braga, "Strain sensor using PCF HiBi fiber". I Encontro Nacional de Física, Foz do Iguaçu, Brazil, 2011.

F.C. Favero, Joel Villatoro, Valerio Pruneri, "All-optical Fiber Interferometric Breathing Sensor"XI Conference on Optical Chemical Sensors and Biosensors, Barcelona-Spain, 2012

Thermal response evaluation of a special fiber sensor

F. C. Fávero, S. M. M. Quintero, Cícero Martelli, Arthur B. Braga and Isabel C. S. Carvalho

Pontifícia Universidade Católica do Rio de Janeiro, Rua Marquês de São Vicente 225, Gávea, 22453-900, Rio de Janeiro, RJ, Brazil

Introduction

High birefringence photonic crystal fibers (HiBi PCF) fibers are often considered to be temperature independent since their birefringence arises from the physical geometry of the core instead of the conventional stress induced refractive index variation in solid HiBi fibers. Although there is a large difference in the temperature dependence of a stress induced HiBi fiber and a HiBi PCF fiber, the HiBi PCF fiber dependence on temperature cannot always be neglected. Applications based on high resolution interferometric devices are a good example. In this case the material thermo optical coefficient plays an important role affecting the determination of the resonant wavelength of the interferometer due to changes in the fiber birefringence.

Theory

The special fiber used was the PM-1550-01 HiBi photonic crystal fiber (from Crystal Fiber). The fiber is made of a solid core surrounded by 6 rings of 2.2μm holes arranged in an 6 fold symmetry, the $d/\Lambda < 0.42$ guarantees its single modeness, where d is the hole diameter and Λ is the pitch between the holes. Two opposite holes of the first ring are substituted by 4.5μm holes in order to induce a symmetry break. This gives rise to birefringence and consequently to two degenerated modes, TE and TM.

In order to study the effect of temperature variations on high birefringence photonic crystal fiber the modal interferometer presented in Figure 1 was assembled. The sensitivity of the fiber birefringence with temperature (K_T) is represented by:

$$K_T = \frac{dn_s}{dT} - \frac{dn_f}{dT} = \frac{dB}{dT} \qquad (1)$$

where $$B = n_s - nf \qquad (2)$$

The phase matching condition variation of the two propagation modes as function of temperature in terms of interfering wavelengths is given by:

$$\frac{d\lambda_m}{dT} = \frac{\lambda_m}{B}\frac{dB}{dT} + \frac{\lambda_m dL}{LdT} \qquad (3)$$

Experimental Procedure

The fiber birefringence was estimated via two different methods. First the group velocity of the two modes, TE and TM, is measured and the phase delay between input and output signals is used to estimate the birefringence via equation (4)

$$B = n_s - n_f = \frac{c\Delta\tau}{L} \qquad (4)$$

Where n_s and n_f correspond to the group indices of the slow and fast modes, $c = 3x10^8\ m/s$ and L is the length of the fiber. A differential group delay $\Delta\tau = 0.39\ ps$ at 1550 nm is obtained, which corresponds to a birefringence value $B = 7.8x10^{-4}$.

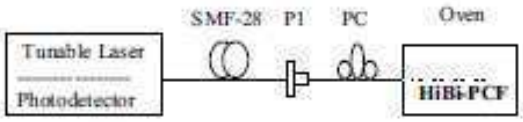

Figure 1. Experimental set-up of the modal interferometer. SM, single mode fiber; P1, polarizer; PC, polarization controller.

The second method used to estimate the fiber birefringence is based on the fringe spacing observed in the spectrum of the modal interferometer (Figure 2) shown in Figure 1. Light from a broad band optical source was launched into the HiBi PCF (9.6cm long) at 45° to the fiber axis exciting equally both polarization eigenmodes. The light reflects at the PCF fiber end tip and the resulting signal is measured by the photodetector. The fiber birefringence can then be calculated using:

$$S = \frac{\lambda^2}{2.L.B} \qquad (5)$$

Where S is the spacing between the minimums in the spectrum,. The estimated birefringence is $B = 8.1 \times 10^{-4}$.

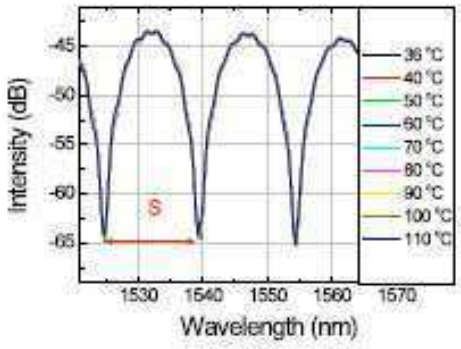

Figure.2 Variation of the spectrum of the modal interferometer with temperature.

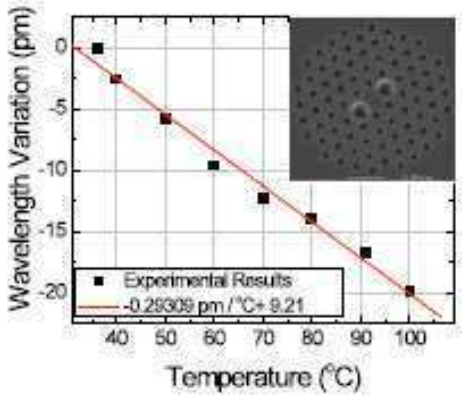

Figure.3. Variation of wavelength (l) with temperature.

In order to characterize the system, the set up described in Figure 2 was used and a piece of 9,6 cm length of PCF sensing element was placed in an electrical furnace, whose temperature was independently monitored by a thermocouple. The investigated temperature range ranged from 30°C to 100°C, and the variation of the wavelength with temperature was of 0.29pm/°C, as shown in Figure 3, the results agree with the literature [1,3,4]

Numerical Simulation

A commercial finite element code (Comsol) was used to model the PCF fiber birefringence dependence with temperature. A two-dimensional, plane-strain state was assumed. The density of the mesh decreased markedly outside the microstrutured region. Nonetheless, nearly 41.000 elements were required to model the PCF. The silica forming the fiber optic was assumed to have an index, n=1.445 (at 1.55μm) and the air holes were assigned an index, n=1. Numerical simulations consisted of two steps: first, the change in refractive index caused by thermal stress was determined. Secondly, the propagation constants, β_{TE} and β_{TM}, were calculated for the distribution of the refraction index over the fiber cross section modified by thermal stresses. The modal field intensity with electric filed polarizations maps for two linear orthogonal polarizations (TE and TM) are presented in Figure 4. The intrinsic birefringence was found to be around $4.7x10^{-4}$. The differences between the calculated and measured values for the fiber birefringence can be accounted for the geometrical perturbation and the residual stress, of the real PCF. Such differences between the real fiber and the model can significantly contribute to such disparities. Birefringence variations due to temperature were not observed. The experimental result showed birefringence variation of order of 10^{-10}/°C, which is out of the precision of Comsol ($1x10^{-6}$).

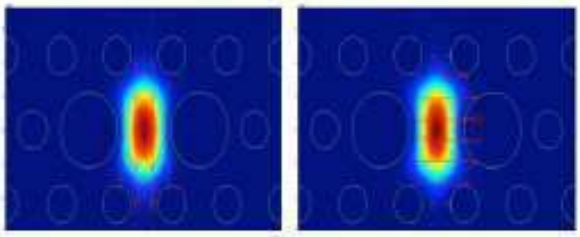

Figure 4. Modal field intensity profile for TE and TM.

Conclusions

The birefringence of a HiBi PCF fiber was estimated via a group delay method and by a method based on the fringe spacing observed in the spectrum of the modal interferometer. The measured birefringence was found to be approximately $B = 8.1x10^{-4}$ which is in good agreement with the values found in the literature. Also, a numerical simulation was performed showing the potential application of the system implemented to evaluate the design and properties of a microstructured fiber for device application.

.

References:

[1] X. Dong, H. Y. Tam, P. Shum, *Appl. Physics Lett. 90, 1511(2007)*

[2] Fiber Optic Communication Systems, G. P. Agrawal, *John Wiley & Sons, INC* (1992)

[3] Y. G. Ham, *Appl. Phys. B, 10, 3350 (2009)*

[4] Do. Hyun. Kim, Jin. U. Kang, *Optics. Express 19, 4490 (2004)*

Photonic Crystal Fiber Pressure Sensor

F. C. Fávero, S. M. M. Quintero, Vinícius V. Silva, Cicero Martelli, Arthur M. B. Braga, Isabel C. S. Carvalho and Roberth W. A. Llerena

Pontifícia Universidade Católica do Rio do Janeiro, Rua Marquês de São Vicente 225, Gávea 22453-900, Rio de Janeiro, RJ, Brazil

ABSTRACT

A high sensitivity optical fiber pressure sensor based on a modal interferometer with high birefringence photonic fiber is proposed and demonstrated. The sensor dependence with hydrostatic pressure is evaluated both numerically and experimentally. The measured pressure sensitivity at room temperature is found to be 3.36 nmMPa^{-1}.

Keywords: Optical fiber sensor, photonic crystal fiber (PCF), modal interferometer, pressure sensor.

1. INTRODUCTION

Optical fiber sensors based upon the enhanced sensitivity of photonic crystal fibers for pressure[1] and strain[2] have been intensively investigated. For instance, Fu and co-workers demonstrated a high sensitivity pressure device (3.46 nm.MPa^{-1}) obtained with a fiber optic pressure transducer based on a polarization maintaining photonic crystal fiber in a Sagnac Interferometer ring[3]. Here, the modal interference of the two orthogonal modes of a HiBi-PCF fiber is used to form an in-fiber interferometer to measure hydrostatic pressure. This sensor scheme has the advantage of being compact whilst still preserving the resonant sensitivity found in interferometric devices as well as the low temperature dependence of the geometrically induced birefringence of the HiBi-PCF fiber. A 2D mechanical analysis of the fiber structure coupled with a 2D vectorial modeling of the fiber modes is carried out in order to further understand the fiber response to hydrostatic pressure. The experimental validation of this structural/electromagnetic model will allow further analysis and developments of specially tailored fibers for pressure sensing.

The sensor sensitivity against hydrostatic pressure relies, ultimately, on the structural and material variations experienced by the fiber under pressure. Such changes will subsequently modify the fiber birefringence through changing the TE and TM modes effective indices ($B = n_{TE} - n_{TM}$). Hence, the fiber birefringence dependence with hydrostatic pressure (K_P) can be written as:

$$K_P = \frac{dn_{TE}}{dP} - \frac{dn_{TM}}{dP} = \frac{dB}{dP} \qquad (1)$$

Where P is the applied pressure and n_{TE} and n_{TM} are the effective refractive indices of the fiber modes. The modal interferometer spectral response as function of pressure can be described as:

$$\frac{d\lambda_m}{dP} = \frac{\lambda_m}{B} K_P + \frac{\lambda_m dL}{LdP} \qquad (2)$$

where L is the length of fiber. With equations (1) and (2) one estimates the effect of the pressure on the fiber's birefringence as well as measure the pressure applied to fiber after some calibration.

2. EXPERIMENTS

The photonic crystal fiber employed as the pressure transducer is the high birefringence PM-1550-01 fiber (from Crystal Fiber, Inc.). The fiber is made of a solid core surrounded by 6 rings of 2.2 μm holes arranged in an 6-fold symmetry, the $d/\Lambda < 0.42$ guarantees its single modeness, where d is the hole diameter and Λ is the pitch between the holes. Two

20th International Conference on Optical Fibre Sensors, edited by Julian Jones, Brian Culshaw, Wolfgang Ecke, José Miguel López-Higuera, Reinhardt Willsch, Proc. of SPIE Vol. 7503, 750364

opposite holes of the first ring are substituted by 4.5 μm holes in order to induce a symmetry break. This gives rise to birefringence and, consequently, to two degenerated modes, TE and TM. In order to study the effect of hydrostatic pressure on the HiBi-PCF, a modal interferometer was assembled as shown in Fig. 1. Light from a tuneable laser source (Micron Optics sm125) is launched into a standard telecom fiber (SMF28). At the SMF28 throughput the signal is coupled into a fiber polarizer and a polarization controller that aligns the light polarization at 45° with the 9.6 cm long PCF fiber axis, thus exciting equally both polarization eigenmodes. The resulting interference signal was measured in reflection by a photodetector integrated into the Micron Optics sm125 interrogator. The sensing PCF fiber has its end face isolated from the external medium by an end-cap keeping, this way, the Fresnel reflection of the fiber/air interface constant[4]. The end cap is made of a capillary fiber (internal hole diameter ~56 μm) which is spliced onto the PCF fiber and has its free end collapsed by an electric arc (inset Fig. 1). The fusion splice of the HiBi-PCF fiber with the SMF28 fiber used a special technique[4] and presented a coupling loss of about 2.0 dB. The main reason for such high losses is the V parameter mismatch between the two fibers. Further processing of the PCF fiber end face should suffice to bring this loss down to less than 1 dB.

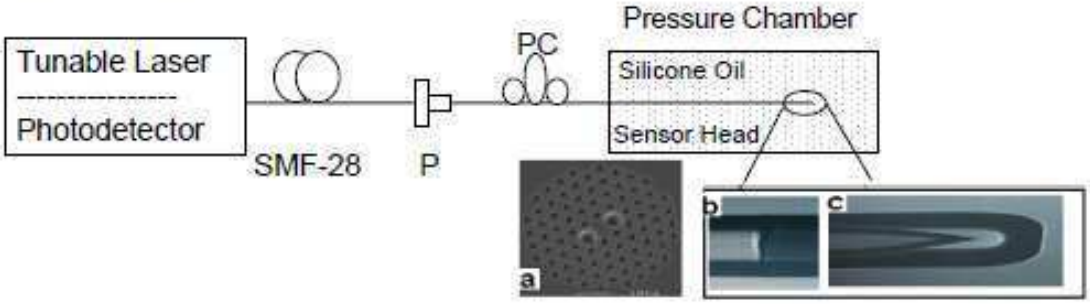

Figure 1. Experimental set-up of the modal interferometer: SMF28: single mode fiber, P: polarizer, PC: polarization controller. Insets: (a) HiBi fiber cross section, (b) Optical image of the splice between the PCF and the standard fiber and (c) fiber end-cap.

To calibrate the device against hydrostatic pressure, the sensor head was placed in a pressure chamber immersed in a controlled temperature silicone oil bath. The maximum applied pressure was 2.42 MPa and the temperature stability of the temperature bath is better than 0.05 °C. Hence, all observed changes in the interferometer spectrum can be inferred as pressure effects.

The PCF fiber birefringence, estimated via the modal interference and observed as an oscillation in the interferometer spectrum, was found to be $B = 8.1\times10^{-4}$ through a simple calculation performed via equation (3) below, where S is the spectral spacing between two minima of the spectrum oscillation. This value was further confirmed by the measurement of differential group delay between the two modes, TE and TM, $\Delta\tau = 0.39$ ps at 1550 nm, which corresponds to a birefringence of $B = 7.8\times10^{-4}$ (see Equation (4) [5]). Both values can be considered equal within the experimental error.

$$S = \frac{\lambda^2}{2LB} \qquad (3)$$

$$B = \frac{c\Delta\tau}{L} \qquad (4)$$

3. RESULTS

The interferometric HiBi-PCF fiber sensor spectral dependence with hydrostatic pressure is presented in Fig. 2 and measured to be linear with an angular coefficient of 3.36 nmMPa^{-1}. This value is very similar to the one previously reported in the literature for this fiber, 3.46 nm.MPa^{-1} [3], showing that sensitivity of the measurement is determined mainly by the sensing fiber. Using equation (1) the fiber birefringence dependence with hydrostatic pressure (K_p) was found to be approximately 1.75×10^{-6} MPa^{-1} (Fig. 3).

A commercially available finite element analysis software (Comsol) was used to model the fiber birefringence dependence with hydrostatic pressure. A two-dimensional, plane-strain state was assumed. Nearly 41,000 elements were required to model the PCF where most of the elements were concentrated around the structured area defining a very fine mesh. The silica forming the optical fiber was assumed to have a refractive index $n = 1.445$ (at 1.55 μm) and the air holes were assigned with an index $n = 1$. The numerical modeling consisted of two basic steps: 1) estimating the changes in the fiber refractive index caused by hydrostatic pressure and 2) determining the propagation constants for the orthogonally polarized modes, β_{TE} and β_{TM}, considering the new distribution of the refraction index across the fiber cross-section induced by external pressure. The distribution of the induced stresses is visualized in terms of Von Mises stress and showed in Fig. 4.a. It is possible to observe how the air holes influence the induced stress distribution and most of the tension is localized around the two larger holes. The modal field distribution for TE is presented in Fig. 4.b. The sensitivity of the modal birefringence to the hydrostatic pressure between the two fundamental modes was calculated according to the equation (1) and found to be linear and approximately $K_P = 1.94\text{x}10^{-6}$ MPa^{-1}, showing consistency with the experimental result ($1.75\text{x}10^{-6}$ MPa^{-1}) calculated using equation (3). The small difference can be credited to the geometrical perturbations in the real PCF fiber which are not reproduced in the idealized numerical model. The experimental and numerical results for the HiBi-fiber birefringence dependence on hydrostatic pressure are plotted in Fig. 3.

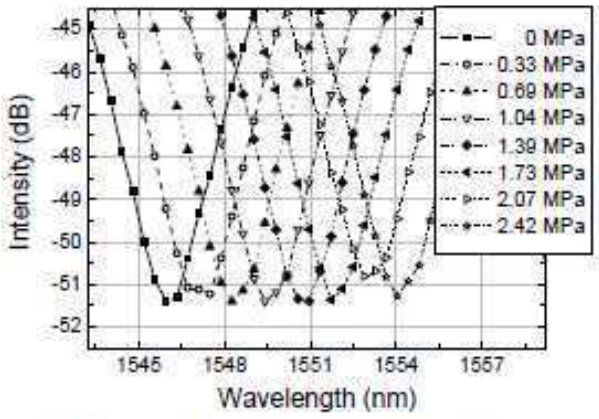

Figure 2. Variations in the spectrum of the modal interferometer due to the applied hydrostatic pressure ranging from 0 to 2.42 MPa.

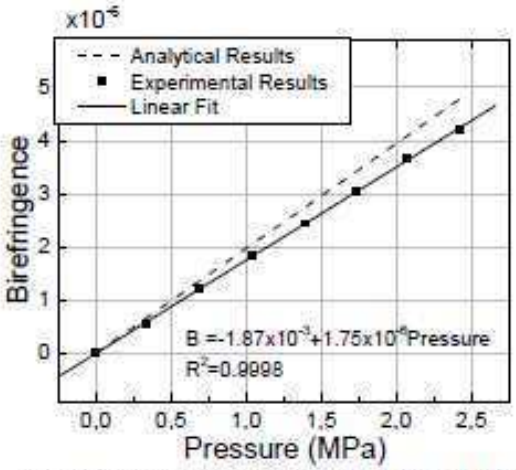

Figure 3. Birefringence variation due to applied pressure. Straight line is a linear fit to experimental data. Dashed line is the numerical modeling.

In spite of the small temperature dependence of the interferometric sensor observed experimentally, the numerical model was unable to show any variation of the phase matching between TE and TM for a large temperature range. The main reason for this is that the software employed to model the fiber has a precision limited to 10^{-6} whilst the temperature dependence is of the order of 10^{-10} °C^{-1}.

4. CONCLUSIONS

A novel sensor scheme using a HiBi-PCF fiber as the sensing element was proposed and demonstrated. The device presents high sensitivity with the applied pressure (3.36 nm.MPa^{-1}), and a rather small cross sensitivity with temperature (0.29 pm/°C). Numerical modeling of the fiber under hydrostatic pressure was performed showing a good agreement with the experimental results. One can, therefore, assume that this numerical method can now be used to design a variety of novel sensing fibers for hydrostatic pressure measurements. The proposed fiber sensor has the advantage over other interferometric schemes, such the Sagnac interferometer, of being simple and ease to manufacture. A drawback, however, is the fact that it operates with polarization which can be very limiting when considering applications at long distances from the interrogation unit. On the other hand, the sensor maximum operating pressure and temperature limits can be quite high, which is interesting for practical applications. In this implementation, due to the mechanical

characteristics of the sensor head, the limiting pressure was 34.5 MPa at 150 °C. However, the range of measurement was limited by the interferometric interrogation method employed here.

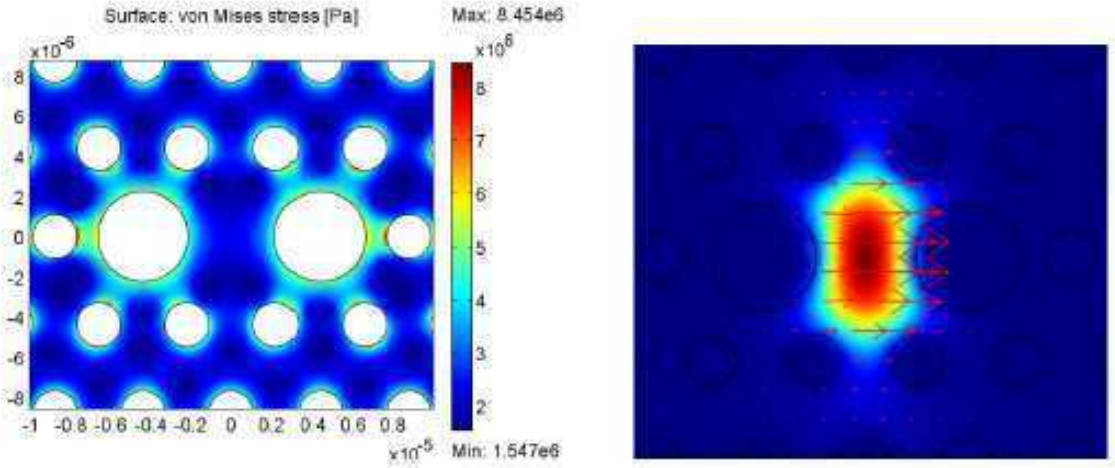

Figure 4. (a) Von Mises stress distribution near the core under hydrostatic pressure (P=2.42 MPa) and (b) TE field intensity profile.

ACKNOWLEDGMENTS

We would like to thank Dr. Walter Margulis from Acreo, Sweden, who kindly supplied the capillary fiber used in this work. We are also thankful for the financial support from the Brazilian Ministry of Science and Technology through CNPq.

REFERENCES

[1] H. Y. Fu, H. Y. Tam, Li-Yhagn Shao, Xinyong Dong, P. K. A. Wai, C. Lu, and Sunil K. Khijwanja, "Pressure sensor realized with polarization-maintaining photonic crystal fiber-based Sagnac Interferometer", Applied Optics, 47, 2835(2008)
[2] Y. G. Ham, "Temperature-insensitive strain using a birefringente interferometer based on a polarization-maintaining photonic crystal fiber", Applied Physics B, 10, 3350 (2009)
[3] Do. Hyun. Kim, Jin. U. Kang "Sagnac loop interferometer based on polarization maintaining photonic crystal fiber with reduced temperature sensitivity", Optics. Express 19, 4490 (2004)
[4] C. Martelli, J. Canning, K. Lyytikainen, N. Groothoff, "Water-core Fresnel fiber", Optics Express 13, 3890 (2005).
[5] G. P. Agrawal, Fiber Optic Communication Systems, John Wiley & Sons, INC, New York (1992)

Photonic crystal fiber and optical microfiber devices based on modes resonance for sensing applications

Guillermo A. CARDENAS-SEVILLA [1, 2], Joel VILLATORO [2], Fernando C. FAVERO [2, 3], Vittoria FINAZZI [2], Valerio PRUNERI [2, 4]

1. Centro de Investigaciones en Optica, A. C. Loma del Bosque #115, Leon, GTO. 37150 Mexico.
2. ICFO – The Institute of Photonic Sciences, Mediterranean Technology Park, Av. del Canal Olimpic s/n, 08860 Castelldefels, Barcelona, Spain.
3. Pontifical Catholic University of Rio de Janeiro, Rua Marquês de São Vicente 225, 22453-900, Rio de Janeiro, RJ, Brazil.
4. ICREA – Institució Catalana de Recerca i Estudis Avançats, 08010, Barcelona, Spain.

Contact name: Guillermo A. Cardenas-Sevilla (memorias@cio.mx).

ABSTRACT

We report the fabrication and characterization of fiber optic devices based on photonic crystal fibers (PCF) and microfibers. These devices have a simple configuration and works using modal interference. The devices are constructed by splicing a small stub a PCF between single mode fibers or by tapering standard single mode fibers together while they are being heated with a high temperature flame torch. The response of the devices and the characterization to surrounded refractive index, temperature, and axial strain are analyzed. The transmission spectrum of these devices exhibit either a single notch or sinusoidal interference patterns which simplifies their analysis.

Key words: Photonic crystal fibers, optical microfibers, passive fiber devices, multiplexing, fiber optic sensors, refractive index sensors.

1.- Introduction

Optical fibers are one of the major technological successes of the 20th century. This technology has developed at an incredible rate. Although communications is the major field of applications, optical fibers have also non-telecom purposes, for example, in beam delivery for medicine, machining and diagnostics, sensing, among other fields. The outcome of photonic crystal fibers (PCF) offers a world of possibilities and perspectives in design and performance for developing new optical fiber-based devices and sensor components [1], [2]. PCFs are novel optical waveguides containing a periodic array of air holes running along the fiber around a solid or hollow core. These fibers have recently attracted great interest in many research areas such as in nonlinear optics and measurement sciences as their manufacturing process allows for a high flexibility in the fiber design. Microfibers, named for their diameters close to or thinner than the wavelength of guided light, have a large core-cladding index contrast for efficient optical confinement, large evanescent fields, strong filed enhancement, and large waveguide dispersions [3-5]. Due to these properties, microfibers find applications in a variety of fields, including photonic devices, optical sensors, and nonlinear optics [6-8].

The aim of this work is to present a series of novel devices based on PCFs and microfibers for sensing applications. PCF devices were built using the microhole collapse effect, where a short piece of PCF is fusion spliced to conventional single-mode fiber (SMF) [9]. The key element of these devices is to control the length of the microscopic zones on which the voids of the PCF are fully col-

lapsed. Also, we present a simple microfiber coupler which exhibits interference pattern with sub-nanometer width fringes and is used as highly sensitive refractometer.

2.- Photonic crystal fiber devices based on modes resonance

Passive and active devices, including filters, couplers, combiners, switches, modulators, etc., are the building block of optical fiber communications systems and sensor networks. Different techniques and phenomena have been proposed or exploited to design a number of devices with conventional optical fibers, see for example [10]. As an alternative to these well-established devices those based on PCF are emerging [11]. By other hand, fiber optic modal interferometry has been around for long as a sensing concept. In the last years modal interferometry saw a huge increase in interest due to the new possibilities offered in this area by the availability of PCF. This circumstance induced a dynamics that keeps rising up to these days [12]. Modal interferometers involve the combination of light of at least two modes that propagate in the fiber. The properties of a PCF modal interferometer to different parameters are determined by the type of interferometer, its geometry, its configuration, and the type of PCF used.

As mentioned above, our devices are based on microhole collapse effect. We fusion spliced a stub of a properly selected index-guiding PCF between two single mode fibers (SMF-28). During the splicing process the voids of the PCF were intentionally collapsed over a controlled microscopic length. According to the collapsed zone and the length of PCF used, different modes were excited and recombined along the PCF length allowing us to design and perform two different devices: a PCF notch filter and a PCF interferometer. The fiber used in our experiments is a cost-effective large-mode-area PCF, commercially known as LMA-10. The cross section of such a fiber is shown in Fig. 1 and its parameters are the following: cores size diameter, 10 μm, average diameter of the voids, 3.1 μm, and average separation between the voids (pitch), 6.6 μm. The external diameter of this PCF is 125 μm which simplifies the splicing with standard single mode fibers. The PCF has six-fold symmetry in the void structure.

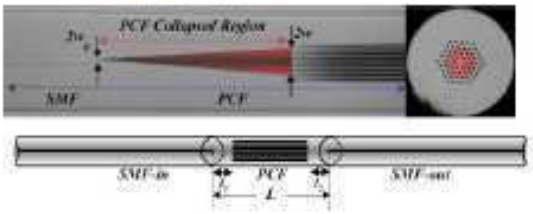

Fig. 1: Micrographs of the PCF and a 200 μm-long collapsed zone. On bottom a schematic of the proposed devices. The broadening of the light spot is illustrated by the circle and cone.

The working principle in our devices is based on the evolution of the propagating beam as it travels from the SMF-in to the PCF and back to the SMF-out. When the fundamental SMF-in mode enters the collapsed region of the PCF it immediately begins to diffract, and consequently, the mode broadens. If w_o is the radius of the light spot at the SMF-in-PCF interface at a wavelength λ, see Fig. 1, then after propagating a length l_1 of collapsed region the radius of the light spot will be:

$$w = w_0\sqrt{1+\left(\lambda l_1/\pi n_f w_0^2\right)^2} \qquad (1)$$

n_f being the refractive index of the collapsed region (solid silica fiber). Under these conditions the PCF will be excited with a Gaussian beam of spot size of $2w$ (see the spot on the PCF in Fig. 1). The mode field mismatch combined with a short section of PCF allows the excitation of a specific cladding mode in the PCF and of course the fundamental HE_{11} core mode. We took advantage of this behavior and we were able to fabricate and characterize the devices proposed below.

2.1.- Photonic crystal fiber notch filter

Wavelength filters are devices that exhibit wavelength-dependent transmittance and are used to block or select a specific wavelength or range of wavelengths, thus playing an important role in optical fiber systems. Here we propose a simple PCF notch filter which is fabricated by splicing a stub of PCF to SMF using the conventional arc discharge technique. A commercial fusion splicing machine (Ericsson FSU 955) was employed to fabricate a collection of samples. A short length of PCF (in the 9-13 mm range) and

collapsed regions with different lengths were found to be crucial. Notch filters with rejection efficiency in excess of 35 dB in the 1500-1600 nm wavelength range were fabricated. Deep notches in the transmission spectra of the devices were observed, some examples are shown in figures 2 and 3.

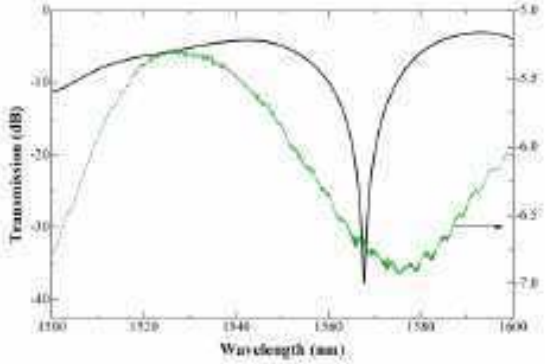

Fig. 2: Transmission spectra of a device when it is in air (solid line) and when it is immersed in index matching oil (dotted line).

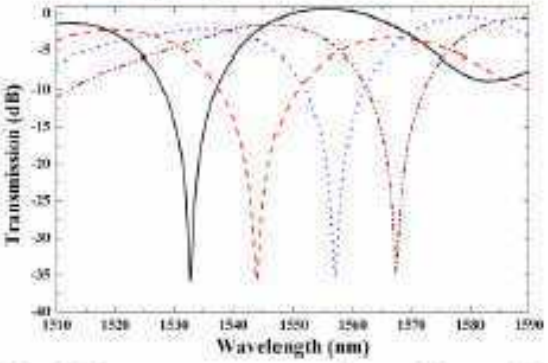

Fig. 3: Transmission spectra of some filters in the 1510-1590 nm wavelength range.

The dips observed in the transmission spectra of our devices are therefore caused by the overlapping between the core and cladding modes referred above. The sinusoidal modulation shown in Fig. 2 was observed when the device was immersed in index matching liquid. This suggests inference between core mode and cladding modes is sensitive to the external environment. Note that in all cases the dips are very narrow and profound. The observed linewidth in all the fabricated notch filters were ~1 nm while the maximum rejection efficiency was in excess of -35 dB.

Owing to the compactness of the filters they can be set in series, thus allowing the filtering of multiple wavelengths. Figure 4 shows the transmission spectrum of two filters when they are independent from each other and also when they are placed in series. We believe that these PCF filters have unique possibilities. From the figure it can be seen that two wavelengths can be filtered simultaneously at the cost of increasing the insertion loss.

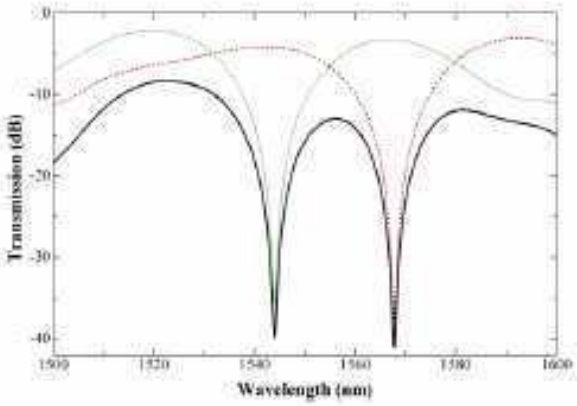

Fig. 4: Transmission spectra of two notch filters were they are independent (dotted lines) and when they are set in series (continuous line).

The sensing properties of individual devices were studied first, particularly to strain and temperature. Basically, these parameters introduce minute changes in the device length or in the modal index which give rise to small changes in the overlapping conditions. As a result, the position of the notches is modified.

The response to axial strain and temperature of the notch filter was studied. These parameters introduce minimal changes in the device length or in the modal index which give rise to small changes in the overlapping conditions. As a result, the position of the notch is modified. Figure 5 shows the observed transmission spectra of a device when it was subjected to axial tensile and compressive strain. The spectra was centered at 1550 nm and subjected to strain (maximum 2500 με). Its position was adjusted in the 1548.4-1552.2 nm range. Temperature dependence of the devices was investigated in the range of 25-250 °C measuring spectral shifts to know how the structural relaxation mechanism under a variation in temperature affects the position of the notch. It can be seen from Fig. 6 that the higher the temperature the longer the notch wavelength. Temperature

sensitivity less then 9 pm/°C, depending on the device length, was found. It was noted that the spectral shifts are only due to thermo-optical behavior. The transmission peak slightly shifted to the longer wavelength in a linear manner.

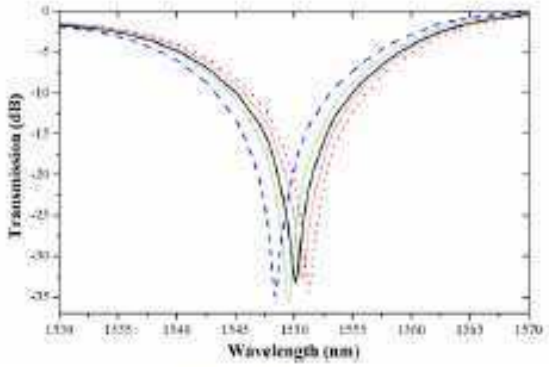

Fig. 5: Transmission spectrum position of a notch filter observed when the device was under axial strian.

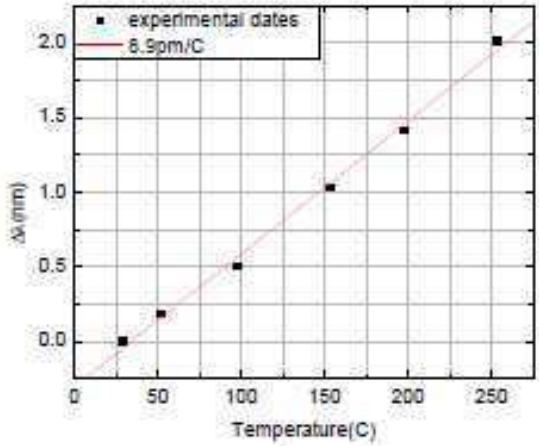

Fig. 6: Position of the notch as function of a change in temperature.

2.2.- Photonic crystal fiber interferometer

Although up to the middle of this decade modal interferometry was supported by standard optical fibers, the outcome of PCFs opened new windows in the optical fibers sensing field; as consequence, a large flux of published works in the last years has been appeared. Those based in the use of the microhole collapsing technique have been widely proposed since it only involves cleaving and splicing which is a process that can be carried out in any fiber-optics laboratory [12]. A compact PCF mode interferometer that operates in reflection mode is proposed for RI sensing. A schematic diagram of the interrogation method used is shown in Figure 7. The device consists of a ~12mm-long stub of commercial photonic crystal fiber (PCF) fusion spliced to standard optical fiber (SMF-28). Two collapsed zones in the PCF allow the excitation and recombination of specific modes. This makes the device reflection spectrum to exhibit interference patterns with extinction ratio of up 40 dB. The measuring range goes from 1.33 to 1.43 which can be measured in two different ways. The shift of the interference pattern or the power at a fixed wavelength can be monitored as a function of the external index, as it can be seen from Fig. 8. In the former case a resolution of 6.5×10^{-5} can be achieved while in the later case it is 6.9×10^{-6}, thanks to the high extinction ratio. We believe that the device proposed here can be useful for industrial applications as well as for biochemical measurement or analysis if the device is coated with layers that sensitive to biological targets.

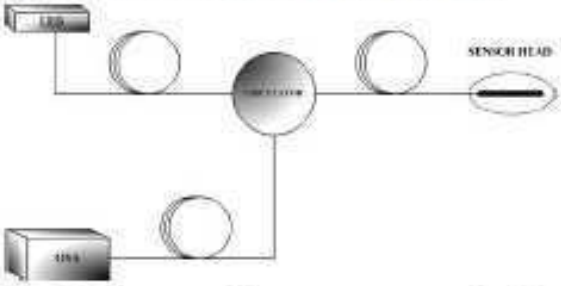

Fig. 7: Schematic of the interrogation method for the sensor proposed.

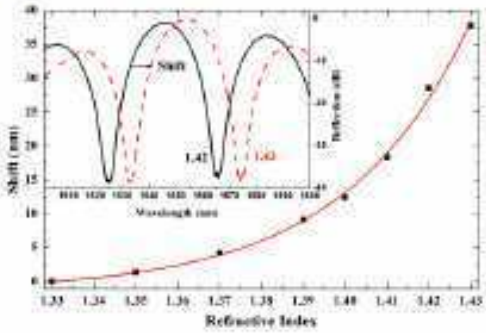

Fig. 8: Shift of the interference pattern as a function of the external index. The inset shows the patterns for two indices.

Temperature modifies the propagation constant of the modes participating in the interference and causes the interference pattern to shift. Thus temperature compensation is usually required. As it can be seen from Fig. 9 our interferometer has a temperature sensitivity of ~8.5 pm/°C and thus temperature

fluctuations of around ~6 °C can be tolerated to achieve the aforementioned resolution.

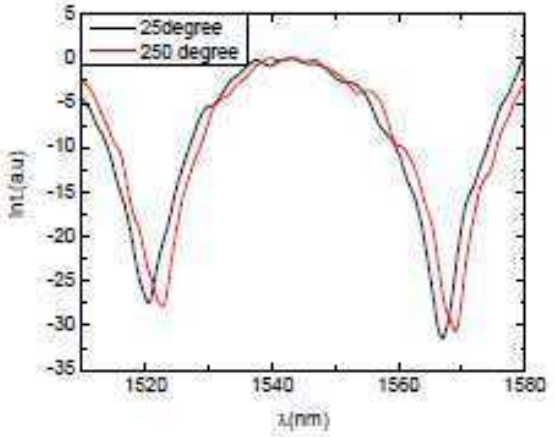

Fig. 9: Interference patterns at two values of temperature.

3.- Optical microfiber coupler

The silica microfiber coupler here presented is fabricated following basically the same method proposed in Ref. [13]. We tapered two twisted standard single mode fibers with a tapering station. The heating source was a flame torch produced by a mixture of oxygen and butane. As can be seen in Fig. 10 the final structure consists of two conical transition tapers and a central uniform waist. In Fig. 11 the output spectrum of the device is showed. This spectrum was obtained by launching a supercontinuum source into the input fibers. The inset shows the interference pattern exhibited by the device over 250 nm. The device had a waist with diameter of 1 μm uniform over 5 mm and was partially embedded in Teflon.

The fibers are adiabatically tapered so that only the fundamental mode is supported. For this reason, the device exhibits an almost sinusoidal pattern due to the beating, or interference, between the two modes of the composite waveguide of the coupler.

To avoid degradation of the device without affecting their optical properties we sandwiched it inside two layers of DuPontTM Teflon AF 1601, where the Teflon layers were spin-coated onto a BK7 wafer. The adopted approach was described by our group in Ref. [6] in order to protect micro-nanofibers. The microfiber is embedded in uniform Teflon layers and is characterized by smooth surfaces. In the central region, the coated microfibers exhibit evanescent field that can be exploited for sensing.

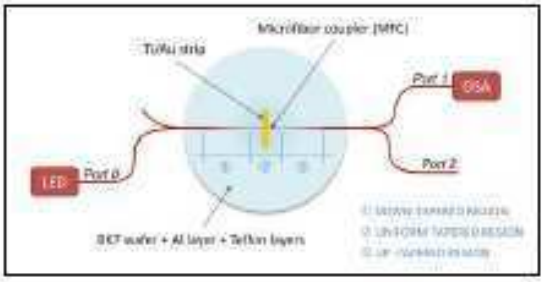

Fig. 10: Schematic of the microfiber coupler and the experimental setup for monitoring the pattern shifts.

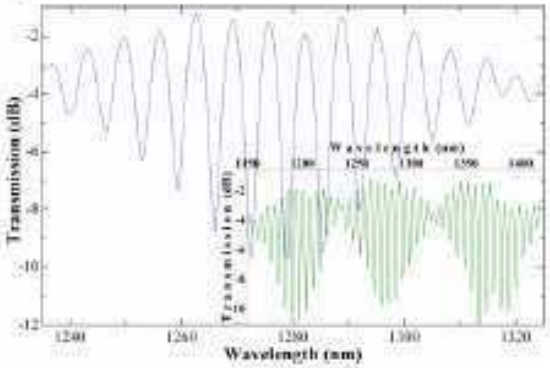

Fig. 11: Zoom in around 1280 nm of the transmission spectrum of a microfiber coupler.

The sensor capabilities of the coupler device were evaluated using solutions with different glucose concentrations and it is showed in Fig. 12 1μl and 90 μl drops of glucose solutions with refractive index varied form 1.33 (pure de-ionized water) to 1.38 were subsequently deposited in the centre of the microfiber coupler using a micropipette. As effect of increasing of the refractive index of the environment surrounding the coupler, the pattern shifts towards long wavelengths. Fig. 12 shows the relationship between the sensor responses and the variations of the refractive index. The sensitivity of the device was 66 nm and 234 nm per refractive index unit for 1ul and 90 ul volume of analyte, respectively.

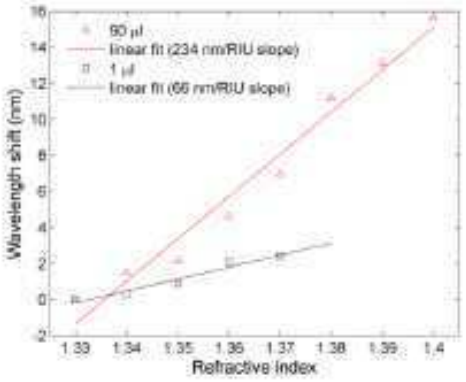

Fig. 13: Refractive-index-dependent shifts of a 1 µm diameter microfiber coupler embedded in Teflon obtained with 1 µl (black squares) and 90 µl (red triangles) of water solutions with different concentration of glucose.

4.- Conclusion

In this work we report on simple photonic devices built with photonic crystal fibers and optical microfibers and their potential sensing applications. By selecting the appropriate collapse length in the splicing process it is possible to fabricate devices based on PCF highly versatile, compact and with high sensitivity. By other hand, a microfiber coupler was presented. The construction of such a device is basically similar to that of fused fiber coupler with the main difference that the microfibers that compose it have subwavelength dimensions. The embedded microfiber coupler showed a good sensitivity to external refractive index changes.

Acknowledgements: This work has been sponsored by...

References

[1] P. St. J. RUSSELL, *"Photonic-crystal fibers"*, IEEE J. Lightw. Technol., 24, 4729-4749, 2006.

[2] O. FRAZAO, J. L. SANTOS, F. M. ARAUJO, and L. A. FERREIRA, *"Optical sensing with photonic crystal fibers"*, Laser Photon. Rev., 2, 449-459, 2009.

[3] R. J. BLACK, F. GONTHIER, J. LAPIERRE, J. BURES, *"Tapered fibers: an overview"*, Proceedings of SPIE, 2-19, 1987.

[4] J. BURES, R. GHOSH , *"Power density of the evanescent field in the vicinity of a tapered fiber"*, J. Opt. Soc. Am. A, 16, 8, 1992-1996, 1999.

[5] L. M. TONG, J. Y. LOU, E. MAZUR, *"Single-mode guiding properties of subwavelength-diameter silica and silicon wire waveguides"*, Opt. Express, 12, 6, 1025-1035, 2004.

[6] N. LOU, R. JHA, J. L. DOMINGUEZ-JUAREZ, V. FINAZZI, J. VILLATORO, G. BADENES, AND V. PRUNERI, *"Embedded optical micro-nano-fibers for stable devices"*,Opt. Lett., 35, 571-573, 2010.

[7] M. SUMETSKY, "Optical micro/nanofibers for sensing applications in *Advanced Photonic Structures for Biological and Chemical Detection*", Springer New York 2009.

[8] S. LEON-SAVAL, T. BIRKS, W. WADSWORTH, P. St. J. RUSSELL, and M. MASON, *"Supercontinuum generation in submicron fibre waveguides"*, Opt. Express, 12, 13, 2864-2869, 2004.

[9] L. XIAO, M. S. DEMOKAN, W. JIN, Y. WANG, and C.-L ZHAO, *"Fusion splicing photonic crystal fibers and conventional single-mode fibers: microhole collapse effect"*, J. Ligthw. Technol., 25, 11, 3563-3574, 2007.

[10] J. P. GOURE, *"Optical fibre devices"*, Institute of Physics Publishing, 2011.

[11] B. EGGLETON, C. KERBAGE, P. WESTBROOK, R. WINDELER, and A. HALE, *"Microstructured optical fiber devices"*, Opt. Express, 9, 698-713, 2001.

[12] J. VILLATORO, V. FINAZZI, G. BADENES, V. PRUNERI, *"Highly sensitivie sensors based on photonic crystal fiber modal interferometers"*, J. Sensors, Article ID 747803, 2009.

[13] Y. JUNG, G. BRAMBILA, and D. J. RICHARDSON, *"Optical microfiber coupler for broadband single-mode operation"*, Opt. Express 17, 5273-5278, 2009.

High-visibility photonic crystal fiber interferometer for ultrasensitive refractometric sensing

Guillermo A. Cárdenas-Sevilla*[a, b], Fernando C. Fávero[b, c], Vittoria Finazzi[b], Joel Villatoro[b], Valerio Pruneri[b, d]

[a]Centro de Investigaciones en Óptica A. C., Loma del Bosque 115, León GTO. 37150 México;
[b]ICFO-Institut de Ciencies Fotoniques, Mediterranean Technology Park, 08860 Castelldefels (Barcelona), Spain;
[c]Pontifical Catholic University of Rio de Janeiro, Rua Marquês de São Vicente 225, 22453-900, Rio de Janeiro, RJ, Brazil;
[d]ICREA-Institució Catalana de Recerca i Estudis Avançats, 08010, Barcelona, Spain

ABSTRACT

A simple and compact photonic crystal fiber (PCF) interferometer that operates in reflection mode is proposed for refractive index (RI) sensing. The device consists of a ~12mm-long stub of commercially available PCF (LMA-10) fusion spliced to standard optical fiber (SMF-28). The device reflection spectrum exhibits interference patterns with fringe contrast up to 40 dB. One of the excited modes in the PCF is sensitive to external RI therefore the device can be useful for refractrometry. The shift of the interference pattern can be monitored as a function of the external index. In the operating range, from 1.33 to 1.43, the maximum shift is less than the interferometer period, so there is no-ambiguity in the measurements. The maximum sensitivity and resolution achieved were 735 nm per RI units and $7x10^{-5}$, respectively. Another approach to measure the external RI consists of monitoring the reflection power located at the quadrature point of the inference pattern in a properly selected wavelength. Consequently the measuring range is narrower but the resolution is higher, up ~$7x10^{-6}$, thanks to the high fringe contrast.

Keywords: Fiber optics sensors, refractive index sensor, photonic crystal fibers, modal interferometry

1. INTRODUCTION

Fiber optic sensors have beneficiated from the developments initially conceived for the optical fiber communications industry[1-4]. These sensors are displacing traditional sensors due to their inherent advantages which include light weight, very small size, immunity to electromagnetic interference, high sensitivity, among others. The monitoring or sensing of the refractive index (RI) with optical fibers is attracting considerable attention by the sensor community. The motivation arises by the fact that different chemical substances and several biological parameters can be detected by means of RI changes. In chemical, food or beverage industries, the monitoring of RI is part of the quality control. In these industries, RI sensors (refractometers) with resolutions in the 10^{-3}-10^{-5} range are sufficient. On the other hand, the detection of minute RI changes is critical in biosensing. For example, molecular bindings, chemical or biochemical reactions are manifested as refractive index changes[5] and refractometric-based sensors capable of resolving RI changes smaller than 10^{-5} are highly desirable[6]. Owing to the broad range of applications aforementioned, there is a growing interest on optical fiber RI sensors or refractometers.

To devise an optical fiber RI sensor one needs access the evanescent waves of the guided light or to excite cladding modes in the fiber since those are sensitive to the surrounding environment. Considerable research effort has been placed on fiber design and mechanism to excite cladding modes. Cladding mode RI sensors based on long-period gratings written in standard fiber[7, 8] or slanted Bragg gratings[9, 10] are compact and highly sensitive. Nevertheless, they require a complex fabrication process or costly read-out units are. The advent of PCFs[11, 12] has also opened new

22nd Congress of the International Commission for Optics: Light for the Development of the World, edited by Ramón Rodríguez-Vera, Rufino Díaz-Uribe, Proc. of SPIE Vol. 8011, 80114K
2011 SPIE · CCC code: 0277-786X/11/$18 · doi: 10.1117/12.901942

possibilities for RI sensing. PCFs offer a number of possibilities in design and performance due to their own structure and their unique properties such as endless single-mode and large-mode area[13]. Index guiding PCFs have a solid core in the fiber center and the cladding consists of a microstructured array of air channels running along the fiber axis. A variation in the channel geometry and a lattice structure offers a large degree of freedom for modifying the optical properties that can not be realized in conventional optical fibers. The confinement of light to the core by modified total internal refraction in PCFs signifies many novel implementations in the field of fiber-optic sensing. There is a growing interest in exploring PCFs for advanced sensor components and devices[14, 15]. The ability to fabricate fibers with unique dispersion profiles and the strong overlap of the optical field with the open-air channels provides potential opportunities for evanescent field sensing and robust devices applications.

Alternatively, one of the areas of greatest interest has been in the development of high-performance interferometric fiber optic sensors. Optical interferometers have played an important role in both fundamental and applied research during the past two centuries. Substantial efforts have been undertaken on Sagnac interferometers, ring resonators, Mach-Zehnder and Michelson interferometers, as well as dual-mode, polarimetric, grating and etalon-based interferometers[3, 16, 17]. Although up to the middle of this decade modal interferometry was supported by standard optical fibers, the outcome of PCFs opened new windows in the optical fibers sensing field; as consequence, a large flux of published works in the last years has been appeared. Those based in the use of the microhole collapsing technique[18-23] have been widely proposed since it only involves cleaving and splicing which is a process that can be carried out in any fiber-optics laboratory.

The properties of a PCF modal interferometer to different parameters are determined by the type of interferometer, its geometry, its configuration, and the type of PCF used. The goal of the new proposes is focus on how to improve the characteristics inherent in a fiber optic sensor such as sensitivity, resolution, size, ranges, among others. In this work, the capability of the in-reflection modal interferometer for bulk external RI detection is proposed. We took the advantages offered by the modal interferometry and the properties of PCFs to build a compact PCF modal interferometer capable to detect refractive index changes of the surrounding medium. The device is fabricated via micro-holes collapsing technique splicing a short section of PCF with single-mode fiber (SMF) and adding a gold mirror in the distal end of the cleaved fiber. Truly sinusoidal and stable interference spectra were observed over a specific wavelength window (1500-1600 nm). A high extinction ratio up to 40 dB for the interference pattern is achieved. The high-visibility of the interference pattern allowed us monitoring the external refractive index changes through a wavelength shift or intensity shift. A sensitivity of 735 nm per RI unit (wavelength codified) and a resolution of 7×10^{-6} measuring the power reflected in the quadrature point (intensity codified) are demonstrated.

2. FABRICATION AND OPERATION PRINCIPLE

Our devices were built using a PCF with six-fold symmetry in the void structure. This fiber is known as large-mode-area PCF (LMA-10), which is commercially available. A drawing of the proposed devices is shown in Fig. 1. The parameters of the PCF are the following: core size diameter, 10μm, average diameter of the voids, 3.1μm, and average separation between the voids (pitch), 6.6μm. The external diameter of this PCF is 125μm which simplifies the splicing process with standard fibers. For the fabrication of the devices, a stub of PCF and standard optical fiber (SMF-28) were spliced with a commercial fusion splicing machine, Ericsson 995-FA. In general, splicing machines join two fibers together by making first a prefusion in which the fibers are cleared by low-level heating. After the prefusion a main fusion process follows in which the two fiber ends are exposed to an intense discharge (high temperature) for a few seconds. During the main fusion process the fiber are pushed and pulled to form a robust and permanent join. The softening point of PCFs is in general lower than that of SMFs due to their holey structure. Thus, if an SMF and a PCF are spliced with a default program for splicing single- or multi-mode fibers the PCF's air holes will entirely collapse over a certain length. In most splicing machines the intensity and duration of the arc discharge of the main fusion process can be adjusted. Thus, one can control the length of the collapsed zone in the PCF[24], allowing us to manage properly the parameters used in the fabrication of the devices.

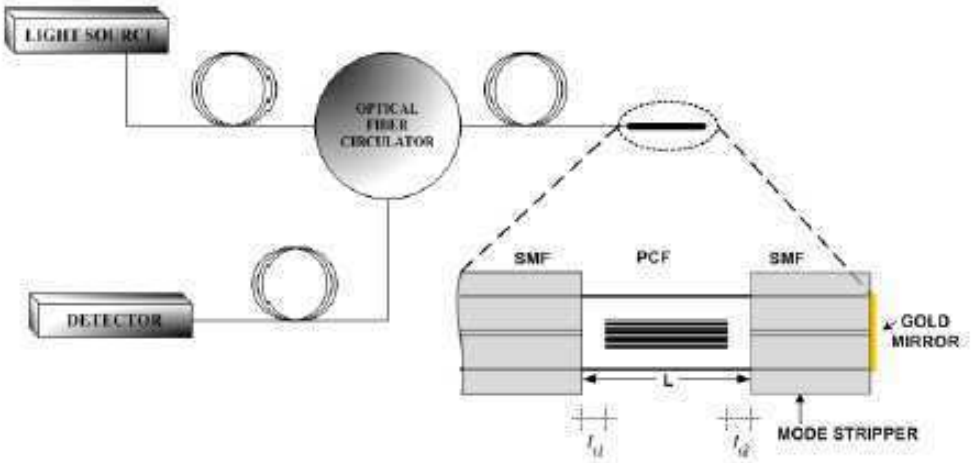

Figure 1. Drawing of the proposed devices and the schematic of its interrogation. L is the PCF length, l_{c1} and l_{c2} are the lengths of the collapsed zones.

The devices proposed falls into the category of single mode-multimode-single mode (SMS) devices, where many variants have been proposed in the literature[25-29]. Depending on the SMS configuration the transmission can exhibit a peak, a dip or a sinusoidal pattern[25-29]. In our case the excitation/overlapping of the modes is carried out with two collapsed zones in the PCF. When the fundamental SMF mode enters the collapsed region of the PCF it immediately begins to diffract, and consequently, the mode broadens. The broadening is also experienced by the excited modes in the PCF when travel to the SMF. If w_0 is the radius of the light spot at the SMF-PCF interface at a wavelength λ, see Fig. 2, then after propagating a length l_{c1} of collapsed region the radius of the light spot will be

$$w = w_0\sqrt{1+\left(\lambda l_1/\pi n_f w_0^2\right)^2}\,, \tag{1}$$

n_f being the refractive index of the collapsed region (solid silica fiber). Under these conditions the PCF will be excited with a Gaussian beam of spot size of $2w$ which is in general larger than the PCF core diameter. Owing to the axial symmetry and the mode field mismatch the excited modes are those that have similar azimuthally symmetry, i.e., the HE_{11} core mode and probably the HE_{22}-like cladding mode. To support the above mechanism, in Fig. 2 we show the calculated longitudinal component of the time-averaged Poynting vector of the HE_{22}-like cladding mode, for a wavelength of λ = 1550nm. From Fig. 2 it can be noted that the field of the HE_{22}-like mode penetrates the entire core mode area; therefore it strongly overlaps with the fundamental HE_{11} core mode.

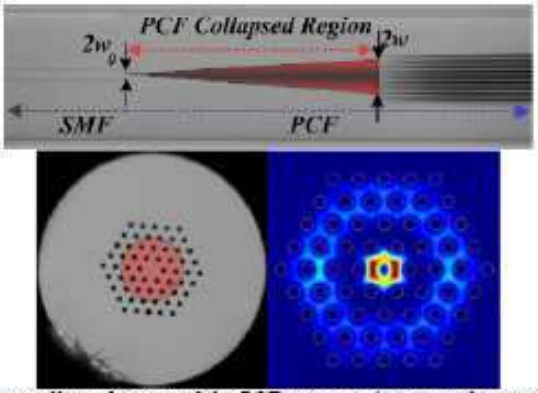

Figure 2. Micrographs a 200 μm-long collapsed zone and the PCF cross section. w_0 and w are described in the text. The HE_{22}-like cladding mode of a LMA-10 calculated at 1550 nm using commercial software COMSOL Multiphysics (showing area equal to 60x60μm).

3. RESULTS AND DISCUSSION

During the fabrication process, we found that when the two collapsed zones had similar lengths, for example, when l_{c1} and l_{c2} were ~160±20μm the reflection spectrum of the devices exhibited sinusoidal interference patterns, see Fig. 3. This behavior is consequence of the recombination of the excited modes in the PCF. To achieve high extinction ratio and to avoid distortion of the interference pattern a section of ~2cm of SMF was left coated and mirrored at the distal end, see Fig. 1. Mode interferometers are sensitive to liquids or coatings deposited on the fiber surface[25, 27]. The interaction of cladding modes with the external index changes their propagation constant, and then, the phase difference. This causes a shift in the interference pattern. To correlate the shift versus the external index in our interferometer the whole length of PCF was immersed in calibrated Cargille oils. Between consecutive measurements the surface of the PCF was cleaned with acetone and ethanol. Figure 3 shows the observed shift in a 12mm-long interferometer as a function of the external index in the 1.33-1.43 range. It can be noted that the shift in that range is ~36 nm, less that the interferometer period, so there is no-ambiguity in the measurements. The shift is more prominent for indices in the 1.41-1.43 range. In this range the sensitivity reaches a value of 735 nm / RIU, where RIU refers to refractive index units. Thus, if a shift of 50 pm of the interference pattern can be resolved the resolution of the device is ~$7x10^{-5}$. This resolution is an order of magnitude higher than that of interferometers built with LMA-8 PCFs[27]. In addition, the present interferometer is three times shorter. The high extinction ratio (in exceeds of 40 dB), the double pass and the types of modes excited in the PCF contribute to the high resolution.

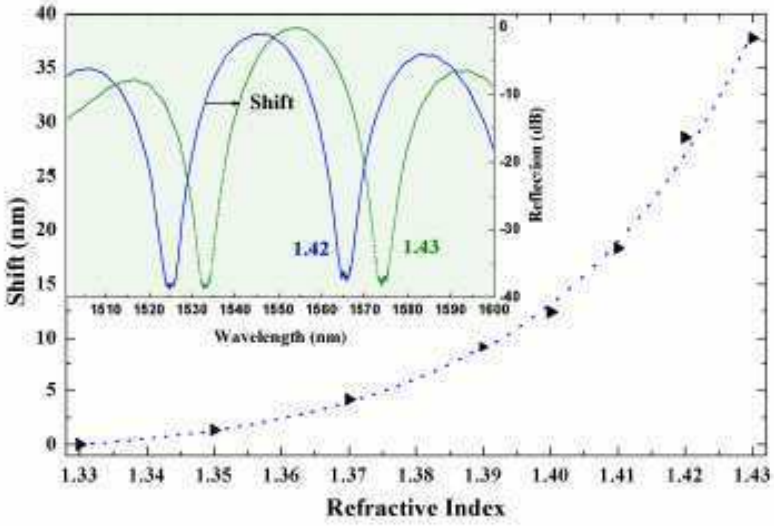

Figure 3. Shift of the interference pattern as a function of the external index. The inset shows the observed patterns when the index was 1.42 or 1.43. The length of the device was 12 mm.

As can be seen in Fig. 4, we made a close up of a minimum of the interference pattern of a 12mm-long interferometer showing three different RI values that are closed to each other. The inset in Fig. 4-(a) shows a reflected interference pattern that can not be standing out at first instance. Making a close up in one of the areas in the reflected spectrum allowed us to see that the shift is minimal but quantifiable. If we want to get a higher sensitivity, this can be achieved with the same device. If we locate the quadrature point (see the arrow in the inset-figure) and monitor the power at a wavelength, in our case λ = 1554.8 nm, and by taking 1.412 as reference, we can see that an increment of $4.9x10^{-4}$ in the refractive index causes a transmission change of nearly 1.4 dB, as it is shown in Fig. 4-(b). Large changes in the reflection are due to the high extinction ratio of the interferometer. Thus, a resolution of $7x10^{-6}$ can be achieved if power changes of 0.01 dB can be resolved, provided that the optical source does not fluctuate during the measurements or that temperature variations have no effect or are compensated.

Temperature fluctuations affect the performance of any sensor and our interferometer is not an exception. The propagation constant of the propagated modes along the fiber and the geometrical dimensions are modified by temperature, which causes a shift in the interference pattern. As a result, the dependence of the interferometer to temperature was studied. A sensitivity of 9 pm / °C was obtained. Thus, temperature fluctuations of around 6 °C can be tolerated to achieve the resolutions mentioned above. It is important to point out that highly stable, single frequency lasers for telecom wavelength range are commercially available. RI measurements in a fixed or controlled temperature environment are also feasible. Therefore, the aforementioned resolutions are reachable. Note that the monitoring the reflected power at a fixed wavelength can be carried out by a simple read-out unit, consisting for example of a laser and a detector, which has a considerable lower cost than complete spectrometers.

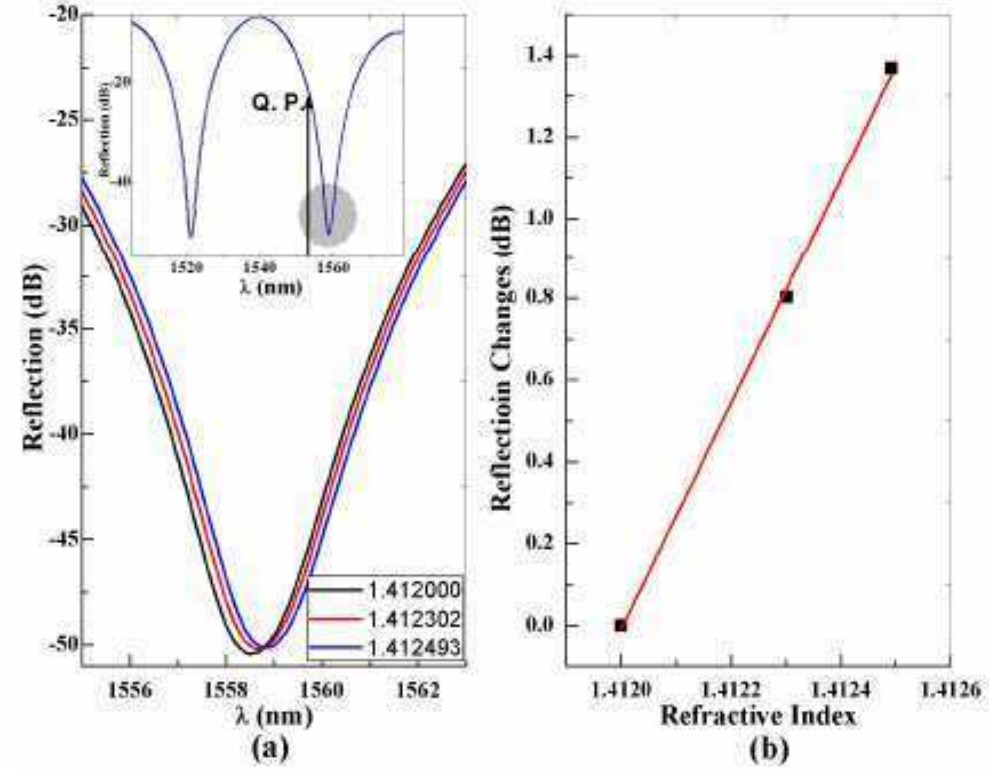

Figure 4. (a) Observed reflection spectra in a 12 mm-long device for three indices indicated in the figure. The inset shows the reflected interference pattern showing the quadrature point located in order to measure the changes in power. (b) Reflection changes as a function of the external refractive index. The monitored wavelength was 1554.8 nm.

4. CONCLUSIONS

In this work we report on simple photonic crystal fiber interferometers for refractive index sensing. Such devices are built by splicing a segment of properly selected PCF between standard optical fibers. During the splice the voids of the PCF are intentionally collapsed over a microscopic region. The collapsed zones introduce a mode field mismatch and allow the excitation and overlapping or recombination of azimuthally symmetric modes in the PCF. As a result, the devices exhibit a sinusoidal interference pattern. The interferometer proposed here is more compact than others based on PCF. In addition, the fringe contrast is around 40 dB, which is higher than that of any other modal interferometer reported until now. The potential in our interferometer for refractometric sensing was demonstrated. The maximum sensitivity, for the 1.42-1.43 range, of a 12 mm-long device was found to be ~735 nm / RIU. Thus, a resolution of ~$7x10^{-5}$ can be achieved if a shift of 50 pm of the interference pattern can be resolved. When the Optical power is monitored (wavelength at the quadrature point) the sensitivity is ~2775 dB/RIU. Thus, a resolution of ~$7x10^{-6}$ can be achieved provided that reflection power changes of 0.01 dB can be resolved. The above

sensitivities and resolutions are possible if the temperature is kept constant. The high resolution is possible for the type modes excited in the PCF and the high fringe contrast. Optimization of the PCF structure may enhance the performance of the devices even further. Thus, the exploitation of the PCF devices here proposed in real applications seems promising. We believe that the interferometer proposed here can be useful for industrial applications as well as for biochemical measurement or analysis if the device is coated with layers that are sensitive to biological targets.

ACKNOWLEDMENTS

G.A.C.S. is grateful to CONACYT (Mexico) for a PhD Fellowship and F.C.F. to the Conselho de Aperfeiçoamento Pessoal de Nivel Superior, (Brazil), processo 251710-8. This work was supported by the Ministerios de Fomento and de Ciencia e Innovación of Spain under projects SOPROMAC No. P41/08 and TEC2010-14832 and the "Ramon y Cajal" program. This research has been partially supported by Fundació Privada Cellex Barcelona.

REFERENCES

[1]. E. Udd, Fiber Optic Sensors: An Introduction for Engineers and Scientists, Wiley, New York, 1991.

[2]. J. Dakin and B. Culshaw, Optical Fiber Sensors: Principles and Components, Vol. 1, Artech, Boston, 1988.

[3]. D. A. Jackson and J. D. C. Jones, [Interferometers] pp. 239-280 in B. Culshaw and J. Dakin Eds., Optical Fiber Sensors: Systems and Applications, Vol. 2, Artech, Norwood, MA, 1989.

[4]. E. Udd, ed., Fiber optics sensors, Proc. SPIE, CR-44 (1992).

[5]. F. Vollmer, D. Braun, A. Libchaber, M. Dhoshsima, I. Teraoka, and S. Arnold, "Protein detection by optical shift of a resonant microcavity" Appl. Phys. Lett. 80, 4057 (2002).

[6]. H. Li and X. Fan, "Characterization of sensing capability of optofluidic ring resonator biosensors" Appl. Phys. Lett. 97, 011105 (2010).

[7]. H. J. Patrick, A. D. Kersey, and F. Bucholtz, "Analysis of the response of long period fiber gratings to external index of refraction", J. Lightwave Technol. 16 (16), 1606-1612 (1998).

[8]. T. Zhu, Y. Song, Y. Rao and Y. Zhu, "Highly sensitive optical refractometer based on edge–written ultra-long-period fiber gratings formed by periodic grooves", IEEE Sens. J., 9 (6), 678-681 (2009).

[9]. T. Guo, H.-Y. Tam, P. A. Drug, and J. Albert, "Reflective tilted fiber Bragg grating refractometer based on strong cladding to core recoupling", Opt. Express, 17 (7), 5736-5742 (2009).

[10]. A. C. L. Wong, W. H. Chung, H.-Y. Tam, and C. Lu, "Single tilted Bragg reflector fiber laser for simultaneous sensing of refractive index and temperature", Opt. Express 19 (2), 409-414 (2011).

[11]. P. St. J. Russell, "Photonic-crystal fibers", J. Lightwave Technol., 24 (12), 4724-4749 (2006).

[12]. J. C. Knight; T. A. Birks, P. St. J. Russell, and D. M. Atkin, "All-silica single-mode fiber with photonic crystal cladding", Opt. Lett. 21 (19), 1547-1549 (1996).

[13]. T. A. Birks, J. C. Knight and P. St. J. Russell, "Endlessly single-mode photonic crystal fiber", Opt. Lett. 22 (13), 961-963 (1997).

[14]. V. P. Minkovich, J. Villatoro, D. Monzon-Hernandez, S. Calixto, A. B. Sotsky, and L. I. Sostkaya, "Holey fiber tapers with resonance transmission for high-resolution refractive index sensing", Opt. Express, 13 (19), 7609-7614, (2005).

[15]. J. M. Fini, "Microstructure fibers for optical sensing in gases and liquids", Meas. Sci. Technol. 15, 1120-1128 (2004).

[16]. J. D. C. Jones, [Interferometry and polarimetry for optical sensing], in Handbook of Optical Fibre Sensing Tehcnology, J. M. Lopez-Higuera Ed., pp 227-245, John Wiley and Sons, West Sussex, UK, (2002).

[17]. F. T. S. Yu and S. Yin, EDs., Fiber Optic Sensors, Marcel and Dekker, New York, USA (2002).